

DAWN: DYNAMIC FRAME AVATAR WITH NON-AUTOREGRESSIVE DIFFUSION FRAMEWORK FOR TALKING HEAD VIDEO GENERATION

Anonymous authors
Paper under double-blind review

ABSTRACT

Talking head generation intends to produce vivid and realistic talking head videos from a single portrait and speech audio clip. Although significant progress has been made in diffusion-based talking head generation, almost all methods rely on autoregressive strategies, which suffer from limited context utilization beyond the current generation step, error accumulation, and slower generation speed. To address these challenges, we present DAWN (**D**ynamic frame **A**vatar **W**ith **N**on-autoregressive diffusion), a framework that enables all-at-once generation of dynamic-length video sequences. Specifically, it consists of two main components: (1) audio-driven holistic facial dynamics generation in the latent motion space, and (2) audio-driven head pose and blink generation. Extensive experiments demonstrate that our method generates authentic and vivid videos with precise lip motions, and natural pose/blink movements. Additionally, with a high generation speed, DAWN possesses strong extrapolation capabilities, ensuring the stable production of high-quality long videos. These results highlight the considerable promise and potential impact of DAWN in the field of talking head video generation. Furthermore, we hope that DAWN sparks further exploration of non-autoregressive approaches in diffusion models. Our code will be publicly available.

1 INTRODUCTION

Talking head generation aims at synthesizing a realistic and expressive talking head from a given portrait and audio clip, which is garnering growing interest due to its potential applications in virtual meetings, gaming, and film production. For talking head generation, it is essential that the lip motions in the generated video precisely match the accompanying speech, while maintaining high overall visual fidelity (Guo et al., 2021a). Furthermore, natural coordination between head pose, eye blinking, and the rhythm of the audio is also crucial for a convincing output (Liu et al., 2023).

Recently, Diffusion Models (DM) (Ho et al., 2020) have achieved significant success in video and image generation tasks (Rombach et al., 2022; Ho et al., 2022b;a; Peebles & Xie, 2023; Ni et al., 2023). However, their application in talking head generation (Shen et al., 2023; Bigioi et al., 2024) still faces several challenges. Although many methods yield high-quality results, most of them rely on autoregressive (AR) (Tian et al., 2024; Ma et al., 2023) or semi-autoregressive (SAR) (Xu et al., 2024c; He et al., 2023) strategies. In each iteration, AR generates one frame, while SAR generates a fixed-length video segment. The two strategies significantly slow down the inference speed and fail to adequately utilize contextual information from future frames, which leads to constrained performance and potential error accumulation, especially in long video sequences (Stypuřkowski et al., 2024; Tian et al., 2024; Xu et al., 2024b).

To address these challenges, we present DAWN (**D**ynamic frame **A**vatar **W**ith **N**on-autoregressive diffusion), a novel approach that significantly improves both the quality and efficiency of talking head generation. Our approach leverages the DM to generate motion representation sequences from a given audio and portrait. These motion representations are subsequently used to reconstruct the video. Unlike other methods, our approach produces videos of arbitrary length in a non-autoregressive (NAR) manner. However, employing the NAR strategy to generate long videos often results in either over-smoothing or significant content inconsistencies due to limited extrapolation (Qiu et al., 2023).

In the context of talking head generation, we suggest that the model’s temporal modeling capability is significantly hindered by the strong coupling relationship among multiple motions. Typically, the motions in talking head include (1) lip motions and (2) head pose and blink movements. The temporal dependency of head and blink movements extends over several seconds, far longer than that of lip motions (Zhou et al., 2020). Training models to capture these long-term dependencies requires extensive sequences, thus increasing the difficulty and cost of training. Fortunately, head and blink movements can be represented as low-dimensional vectors (Zhang et al., 2023), enabling the design of a lightweight model that learns these long-term dependencies by training on extended sequences. Thus, to further enhance the temporal modeling and extrapolation capabilities of DAWN, we disentangle the motion components involved in talking head videos. Specifically, we use the Audio-to-Video Flow Diffusion Model (A2V-FDM) to learn the implicit mapping between the lips and audio, while generating the head pose and blinks via explicit control signals. Additionally, we propose a lightweight Pose and Blink generation Network (PBNet) trained on long sequences, to generate natural pose/blink movements during inference in a NAR manner. In this way, we simplify the training of A2V-FDM as well as achieve the long-term dependency modeling of the pose/blink movement. To further strengthen the convergence and extrapolation capabilities of A2V-FDM, we propose a two-stage training strategy based on curriculum learning to guide the model in generating accurate lip motion and precise pose/blink movement control.

The main contributions of this work are as follows: 1) We present DAWN (**D**ynamic frame **A**vatar **W**ith **N**on-autoregressive diffusion) for generating dynamic-length talking head videos from portrait images and audio clips in a non-autoregressive (NAR) manner, achieving faster inference speeds and high-quality results. To the best of our knowledge, this is the first NAR solution based on diffusion models designed for general talking head generation. 2) To compensate for the limitations of extrapolation in NAR strategies and enhance the temporal modeling capabilities for long videos, we decouple the motions of the lips, head, and blink, achieving precise control over these movements. 3) We propose the Pose and Blink generation Network (PBNet) to generate natural head pose and blink sequences exclusively from audio in a NAR manner. 4) We introduce the Two-stage Curriculum Learning (TCL) strategy to guide the model in mastering lip motion generation and precise pose/blink control, ensuring strong convergence and extrapolation ability.

2 RELATED WORKS

Audio-driven talking head generation. Initial approaches for talking head generation employed deterministic models to map audio to video streams (Fan et al., 2016), with later methods introducing generative models such as GANs (Isola et al., 2016a), VAEs (Kingma & Welling, 2022), and diffusion models (DMs) (Ho et al., 2020). GAN-related methods (Vougioukas et al., 2020; Pumarola et al., 2018; Hong et al., 2022) improved visual realism but faced convergence and mode collapse issues (Xia et al., 2022). Following this, VAEs (Kingma & Welling, 2022) generated 3D priors like 3D Morphable Models (3DMM) (Bianz & Vetter, 1999) followed by high-fidelity rendering (Ren et al., 2021), which limited the realism and vividness. In contrast, DMs have been introduced into talking head generation due to their good convergence, excellent generation performance, and diversity. Stypułkowski et al. (2024) presented a DM-based talking head generation solution using an AR strategy to generate videos frame-by-frame iteratively. Subsequently, Tian et al. (2024) improved this AR strategy by incorporating motion conditions extracted by a VAE-based network as priors for each iteration, effectively mitigating degradation issues. Concurrently, Xu et al. (2024c); He et al. (2023) advocated for motion modeling instead of image modeling. They utilized DMs to iteratively generate latent motion representations over a fixed number of frames in a SAR manner, subsequently converting these motion representations into video frames. While most diffusion-based methods produce promising results, their AR or SAR strategies incur slow generation speeds and collapse in long-video generation. Although methods like Tian et al. (2024); Xu et al. (2024c) alleviate issues such as inconsistencies in content across iterations and long video generation collapse, the risk of error accumulation remains unresolved. While methods like Du et al. (2023) use identity-specific NAR strategies, to the best of our knowledge, none have addressed NAR talking head generation for arbitrary identities. Consequently, we propose a novel NAR dynamic frame generation framework based on DM, which aims to achieve the low-cost and high-quality rapid generation of realistic talking head video through a clip of audio and arbitrary portrait.

Audio-driven pose and blink generation. Head pose and blink movements significantly impact the naturalness of talking head videos. However, the mapping from audio to pose and blink movement is a one-to-many problem, which presents a significant challenge (Xu et al., 2024a; Chen et al., 2020). Early works primarily focused on controlling poses directly using facial landmarks or video references (Zhou et al., 2021; Guo et al., 2021b). However, these approaches require additional guidance information, which impairs the diversity of the results. Later studies considered generating both pose and blink within the context of talking head generation (Zhou et al., 2020). However, simultaneously generating all facial movements can cause interference and ambiguity (Zhang et al., 2023). Therefore, some works attempted to decouple the speaker’s actions into components like lip, head pose, and blink, using discriminative models to predict these conditions separately (Wang et al., 2021; He et al., 2023). Later, researchers recognized that probabilistic modeling is better suited for the one-to-many mapping relationship, leading to the proposal of a VAE-based pose generation framework (Liu et al., 2023). However, most existing pose generation strategies also depend on AR or SAR approaches, negatively impacting efficiency, smoothness, and naturalness. To address these issues, we design a VAE-based NAR pose generation method to produce vivid and smooth pose and blink movements while maintaining the NAR generation of the entire framework.

3 METHOD

As shown in Figure 1, DAWN is divided into three main parts: (1) the Latent Flow Generator (LFG); (2) the conditional Audio-to-Video Flow Diffusion Model (A2V-FDM); and (3) the Pose and Blink generation Network (PBNet). First, we train the LFG to estimate the motion representation between different video frames in the latent space. Subsequently, the A2V-FDM is trained to generate temporally coherent motion representation from audio. Finally, PBNet is used to generate poses and blinks from audio to control the content in the A2V-FDM. To enhance the model’s extrapolation ability while ensuring better convergence, we propose a novel Two-stage Curriculum Learning (TCL) training strategy. We will first discuss preliminaries, then present the specific details of DAWN’s three main components, namely LFG, A2V-FDM, and PBNet in Sections 3.2, 3.3, and 3.4, respectively. Finally, we will introduce the TCL strategy in Section 3.5.

3.1 PRELIMINARIES

Task definition. The task of talking head generation involves creating a natural and vivid talking head video from two inputs: a static single-person portrait, \mathbf{x}_{src} , and a speech sequence, $\mathbf{y}_{1:N} = \{\mathbf{y}_0, \mathbf{y}_1, \dots, \mathbf{y}_N\}$. The static image \mathbf{x}_{src} and the speech sequence \mathbf{y} can originate from any individual, and the output is $\hat{\mathbf{x}}_{1:N} = \{\hat{\mathbf{x}}_0, \hat{\mathbf{x}}_1, \dots, \hat{\mathbf{x}}_N\}$, where N represents the total number of frames.

Diffusion models. Diffusion models generate samples conforming to a given data distribution by progressively denoising Gaussian noise (Ho et al., 2020). Let \mathbf{x}_0 represent data sampled from a given distribution $q(\mathbf{x}_0)$. In the forward diffusion process, Gaussian noise is progressively added to \mathbf{x}_0 after T steps, resulting in noisy data \mathbf{x}_T (Nichol & Dhariwal, 2021; Song et al., 2020), and the conditional transition distribution at each step is defined as:

$$q(\mathbf{x}_t|\mathbf{x}_0) = \mathcal{N}(\mathbf{x}_t; \sqrt{\bar{\alpha}_t} \mathbf{x}_0, (1 - \bar{\alpha}_t)\mathbf{I}) \quad (1)$$

where $\bar{\alpha}_t = \prod_{i=1}^t \alpha_i$. The reverse diffusion process gradually recovers the original data from the Gaussian noise $\mathbf{x}_T \sim \mathcal{N}(0, I)$, utilizing a neural network to predict $p_\theta(\mathbf{x}_{t-1}|\mathbf{x}_t)$, where θ represents the parameters of the neural network. The model is trained using the following loss function:

$$L_{\text{simple}} = \mathbb{E}_{\mathbf{t}, \mathbf{x}_0, \epsilon} [\|\epsilon - \epsilon_\theta(\mathbf{x}_t, t)\|^2] \quad (2)$$

where ϵ is the Gaussian noise added to \mathbf{x}_0 in the forward diffusion process to obtain \mathbf{x}_t , and $\epsilon_\theta(\mathbf{x}_t, t)$ is the noise predicted by the model. In video-related tasks, the denoising model can be implemented via a 3D U-Net (Ho et al., 2022b; Çiçek et al., 2016).

3.2 LATENT FLOW GENERATOR

The Latent Flow Generator (LFG) is a self-supervised training framework designed to model motion information between the source image \mathbf{x}_{src} and the driving image \mathbf{x}_{dri} . As illustrated in Figure 1 (a), LFG consists of three trainable modules: the image encoder \mathcal{E} , the flow predictor \mathcal{P} , and the image

162
163
164
165
166
167
168
169
170
171
172
173
174
175
176
177
178
179
180
181
182
183
184
185
186
187
188
189
190
191
192
193
194
195
196
197
198
199
200
201
202
203
204
205
206
207
208
209
210
211
212
213
214
215

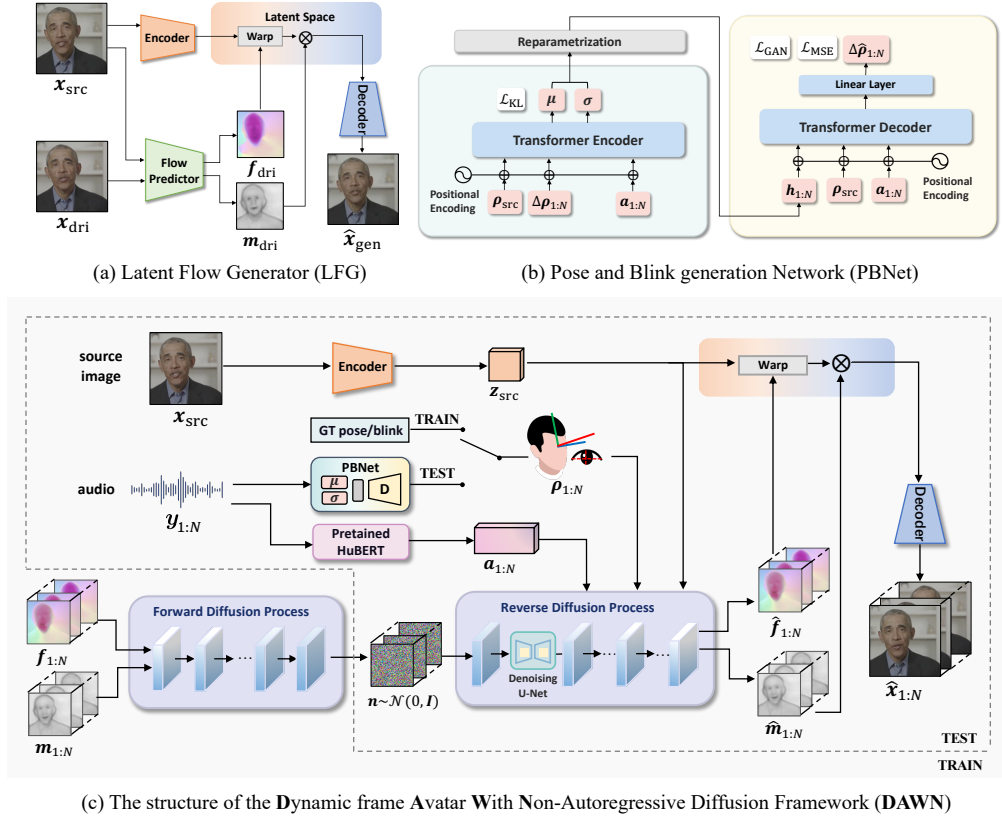


Figure 1: The pipeline of DAWN. First, we train the Latent Flow Generator (LFG) in (a) to extract the motion representation from the video. Then the Pose and Blink generation Network (PBNet) in (b) is utilized to generate the head pose and blink sequences of the avatar. Subsequently, the Audio-to-Video Flow Diffusion Model (A2V-FDM) in (c) generates the talking head video from the source image conditioned by the audio and pose/blink sequences provided by the PBNet.

decoder \mathcal{D} . During training, $\mathbf{x}_{\text{src}}, \mathbf{x}_{\text{dri}} \in \mathbb{R}^{H \times W \times 3}$ are images randomly selected from the same video. The image encoder \mathcal{E} encodes the source image \mathbf{x}_{src} into a latent code $\mathbf{z}_{\text{src}} \in \mathbb{R}^{H_z \times W_z \times C_z}$. The flow predictor estimates a dense flow map \mathbf{f} and a blocking map \mathbf{m} (Siarohin et al., 2021; 2020), corresponding to \mathbf{x}_{src} and \mathbf{x}_{dri} :

$$\mathbf{f}, \mathbf{m} = \mathcal{P}(\mathbf{x}_{\text{src}}, \mathbf{x}_{\text{dri}}) \quad (3)$$

The flow map $\mathbf{f} \in \mathbb{R}^{H_z \times W_z \times 2}$ describes the feature-level movement of \mathbf{x}_{dri} relative to \mathbf{x}_{src} in horizontal and vertical directions. The blocking map $\mathbf{m} \in \mathbb{R}^{H_z \times W_z \times 1}$ ranging from 0 to 1, indicates the degree of area blocking in the transformation from \mathbf{x}_{src} to \mathbf{x}_{dri} . The flow map \mathbf{f} is used to perform the affine transformation \mathcal{A} , serving as a coarse-grained warping of \mathbf{z}_{src} . Subsequently, the blocking map \mathbf{m} guides the model in repairing the occlusion area, thereby serving as fine-grained repair. Finally, the image decoder \mathcal{D} converts the warped latent code into the target image $\hat{\mathbf{x}}_{\text{gen}}$, where the \otimes is the element-wise product:

$$\hat{\mathbf{x}}_{\text{gen}} = \mathcal{D}(\mathcal{A}(\mathbf{z}_{\text{src}}, \mathbf{f}) \otimes \mathbf{m}) \quad (4)$$

The LFG is trained in an unsupervised manner and optimized using the following reconstruction loss:

$$L_{\text{LFG}} = L_{\text{rec}}(\hat{\mathbf{x}}_{\text{gen}}, \mathbf{x}_{\text{dri}}) \quad (5)$$

where L_{rec} is a multi-resolution reconstruction loss derived from a pre-trained VGG-19 network, used to evaluate perceptual differences between $\hat{\mathbf{x}}_{\text{gen}}$ and \mathbf{x}_{dri} (Johnson et al., 2016). We consider the concatenation of \mathbf{m} and \mathbf{f} as $\mathbf{z}^m = [\mathbf{f}, \mathbf{m}]$ to represent the motion of \mathbf{x}_{dri} relative to \mathbf{x}_{src} . In this

way, we achieve two objectives: 1) finding an effective explicit motion representation z^m , which is identity-agnostic and well-supported by physical meaning, and 2) reconstructing x_{dri} from x_{src} and z^m without the need for a full pixel generation.

3.3 CONDITIONAL AUDIO2VIDEO FLOW DIFFUSION MODEL

Through the LFG in Section 3.2, we can specify a x_{src} , and extract the identity-agnostic motion representations $z_{1:N}^m$ of the talking head video clip $x_{1:N}$ as well as the latent code z_{src} extracted by \mathcal{E} from x_{src} . Therefore, we design the A2V-FDM to generate the motion representations $\hat{z}_{1:N}^m = [\hat{f}_{1:N}, \hat{m}_{1:N}]$ of each frame relative to x_{src} :

$$\hat{z}_{1:N}^m = \text{DM}(\mathcal{E}(x_{\text{src}}), y_{1:N}, \rho_{1:N}) \quad (6)$$

where the DM refers the diffusion model and $\rho_{1:N}$ is the pose/blink signal. After generating $\hat{z}_{1:N}^m$, we use the decoder \mathcal{D} in LFG to reconstruct the $\hat{z}_{1:N}^m$ to the target video frames, via the Equation 4. The structure of A2V-FDM is illustrated in Figure 1 (c). The A2V-FDM model includes a 3D U-Net denoising backbone (Ho et al., 2022b). The residue block in the 3D U-Net contains temporal attention and spatial attention modules, which handle frame-level and pixel-level dependencies respectively. The parameters of the temporal attention module are independent of the input length, so we believe that 3D U-Net can theoretically process video sequences of any length. However, to ease training difficulty, we train on short sequences and aim for long-sequence inference. To enhance the 3D U-Net’s extrapolation ability when handling long sequences, we used Rotary Positional Encoding (RoPE) (Su et al., 2023) instead of traditional absolute position embeddings in the temporal attention module.

Conditioning. We incorporate the following conditions to control its generative behavior: audio embedding $a_{1:N}$, pose/blink signal $\rho_{1:N}$, and source image latent code z_{src} . The audio embedding $a_{1:N}$, extracted from the audio $y_{1:N}$ using Hubert (Hsu et al., 2021), implicitly controls the lip motion. Due to the strict alignment with video frames, we apply the audio embedding to its corresponding image. Additionally, the avatar’s pose and blink are controlled via explicit signals. The pose is described by a 6D vector Ji et al. (2022). During training, the pose is extracted from video using an open-source tool (Guo et al., 2020). For the blink signal, we adopt the aspect ratio of the left and right eyes, following (Zhang et al., 2023). To account for the arbitrary pose and eye-opening degree of the source image x_{src} , we use the difference between the current frame x_i and the source frame x_{src} : $\Delta\rho_i = \rho_i - \rho_{\text{src}}$, which models the transition of state rather than the state itself. The model is provided with features z_{src} to supply facial visual details. Each frame’s latent code performs cross attention with the audio embedding a_i and pose/blink information $\Delta\rho_i$, respectively. This process injects these conditions into the latent code with different spatial weights, controlling specific regions of the generated content. The image feature z_{src} is regarded as a global condition and is concatenated directly with the noisy data as the initial input to the 3D U-Net. We also utilize landmarks to create a face region mask for x_{src} , embedded with a lightweight convolutional network, similar to the approach by Tian et al. (2024). This mask adds to the denoising process in the same manner as z_{src} .

Loss function. We employed the DM regular denoising loss, L_{simple} , in Equation 2 to train our model. The synchronization of lip motions with audio is crucial for the talking head task, while the lips often constitute only a small portion of the frame. Consequently, during training, we employed landmarks to isolate the lip region by generating a lip mask, m_{lip} . We then applied an additional weight, w_{lip} , to the denoising process of this region, similar to Stypułkowski et al. (2024). Ultimately, our loss function is defined as:

$$L = L_{\text{simple}} + w_{\text{lip}} \cdot (L_{\text{simple}} \otimes m_{\text{lip}}) \quad (7)$$

where the symbol \otimes denotes element-wise product.

3.4 AUDIO-DRIVEN POSE AND BLINK GENERATION

To prevent the generated results from exhibiting overly monotonous and minimal movements, we design a separate module, namely the Pose and Blink generation Network (PBNet). As shown in Figure 1 (b), PBNet learns the mapping between audio and pose/blink movements. To maintain the non-autoregressive (NAR) generation capabilities of A2V-FDM, PBNet employs a transformer-based Variational Autoencoder (VAE) (Petrovich et al., 2021) to generate variable-length pose and blink

sequences. The inputs to PBNet include the initial pose/blink state ρ_{src} , the residual pose/blink $\Delta\rho_{1:N}$, and the audio embedding $\mathbf{a}_{1:N}$. The transformer encoder \mathcal{E}_t embeds these inputs into a Gaussian-distributed and obtain latent code $\mathbf{h} \in \mathbb{R}^{N \times C_h}$ through resampling :

$$\boldsymbol{\mu}, \log\boldsymbol{\sigma} = \mathcal{E}_t(\rho_{\text{src}}, \Delta\rho_{1:N}, \mathbf{a}_{1:N}), \text{ s.t. } \mathbf{h} \sim \mathcal{N}(\boldsymbol{\mu}, \boldsymbol{\sigma}) \quad (8)$$

We design \mathbf{h} to have the same length as $\Delta\rho$ to ensure it can carry sufficient information for variable-length inputs. The transformer decoder \mathcal{D}_t generates the final pose/blink sequence $\Delta\hat{\rho}_{1:N}$, conditioned on $\mathbf{a}_{1:N}$ and ρ_{src} :

$$\Delta\hat{\rho}_{1:N} = \mathcal{D}_t(\mathbf{h}, \mathbf{a}_{1:N}, \rho_{\text{src}}) \quad (9)$$

To enhance the model’s extrapolation capability, we use RoPE as the positional encoding in the decoder, consistent with A2V-FDM. During training, we apply an MSE-based reconstruction loss L_{rec} and an adversarial loss L_{GAN} to guide the model in completing basic reconstruction tasks (Isola et al., 2016a; Ginosar et al., 2019). Additionally, we employ a KL divergence loss L_{KL} to ensure that the latent code \mathbf{h} closely approximates a standard Gaussian distribution.

3.5 TWO-STAGE CURRICULUM LEARNING FOR TALKING HEAD GENERATION

Empirical evidence indicates that training our A2V-FDM model solely with fixed-length short video clips leads to inaccurate control of poses and blinks, as well as poor generalization to longer videos. We argue that a one-step training approach impedes the model’s convergence to an optimal solution and fails to achieve satisfactory results in the complex task of talking head generation. To address these issues, we propose an innovative Two-Stage Curriculum Learning (TCL) strategy inspired by the theory of curriculum learning (Bengio et al., 2009).

Overall, the goal of the A2V-FDM during the training process can be expressed as:

$$\hat{\mathbf{x}}_{1:N} = \mathcal{D}(\text{DM}(\mathcal{E}(\mathbf{x}_{\text{src}}), \mathbf{y}_{1:N}, \rho_{1:N})) \quad (10)$$

In the first stage, we set $\mathbf{x}_{\text{src}} = \mathbf{x}_1$, and the sequence length $N = K'$ is a fixed, relatively small constant. This stage primarily focuses on enabling the model to generate basic lip motions. However, utilizing \mathbf{x}_1 as the source image often exhibits limited variations in poses and blinks, and using short clips can result in a scarcity of training samples with significant pose or blink movements. Therefore, in the second stage, we set $\mathbf{x}_{\text{src}} \in \mathbb{X}$ randomly, where \mathbb{X} is the set of frames in the entire video, to learn control capabilities of large pose transformation. Additionally, differing from stage one, we randomly set $N \in [K_{\text{min}}, K_{\text{max}}]$, $K_{\text{min}} > K'$. This approach aims to enhance control over poses and blinks while maintaining precise lip motions, as longer clips contain more diverse pose and blink movements. Training with random-length sequences also helps the model avoid a bias towards fixed-length sequences, further enhancing the model’s extrapolation.

3.6 INFERENCE

Our inference process has four steps: 1) Extract the audio embedding $\mathbf{a}_{1:N}$. 2) Use the source image \mathbf{x}_{src} to extract the initial pose/blink state ρ_{src} for PBNet. Along with $\mathbf{a}_{1:N}$ and a latent space vector $\mathbf{h}_{1:N}$ sampled from a standard Gaussian distribution, PBNet generates the pose/blink sequences $\hat{\rho}_{1:N}$. 3) Input \mathbf{x}_{src} , $\mathbf{a}_{1:N}$, and $\hat{\rho}_{1:N}$ into the A2V-FDM, which generates the motion representation sequences $\hat{\mathbf{z}}_{1:N}^m$. 4) Finally, decode the video sequence $\hat{\mathbf{x}}_{1:N}$ from \mathbf{x}_{src} and $\hat{\mathbf{z}}_{1:N}^m$. **Both PBNet and A2V-FDM generate sequences of dynamic length in a single pass, depending on input audio length.**

Our method leverages non-autoregressive (NAR) generation during the inference process. To enhance extrapolation during inference, we utilize local attention (Luong, 2015) in the temporal attention module for both the PBNet decoder and the 3D U-Net in A2V-FDM, which restricts the attention scores to a local region. This approach effectively models local dependencies in talking head videos. To accommodate the different temporal dependencies of lip motions and pose/blink movements, we use a larger window size in the local attention mechanism of PBNet compared to A2V-FDM.

4 EXPERIMENT

4.1 SETUP

Dataset. Our method is evaluated on two datasets: CREMA (Cao et al., 2014) and HDTF (Zhang et al., 2021). The CREMA dataset was collected in a controlled laboratory environment and contains

7,442 videos from 91 identities, with durations ranging from 1 to 5 seconds. The HDTF dataset consists of 410 videos, with an average duration exceeding 100 seconds. These videos are gathered from wild scenarios and feature over 10,000 unique sentences for speech content, along with diverse head pose movements. We partitioned the CREMA dataset into training and testing sets following Styplkowski et al. (2024). As for the HDTF dataset, we conducted a random split with a 9:1 ratio between the training and testing sets. We resized the videos at a resolution of 128×128 and a frame rate of 25 frames per second (fps) without any additional preprocessing.

Implementation details. The architecture of the encoder and decoder in our model aligns with the design proposed by Johnson et al. (2016), while the flow predictor is implemented based on MRAA (Siarohin et al., 2021). The PBNet model is trained using pose and blink movement sequences of 200 frames. During the inference phase of the PBNet model, a local attention mechanism with a window size of 400 is employed. For the inference phase of the A2V-FDM model, local attention with a window size of 80 is applied. In our evaluation, the length of one-time inference for CREMA is dynamic and depends on the ground truth, while for HDTF, it is fixed at 200 frames for better comparison.

Evaluation metrics. We evaluate the performance of our method using various metrics. Specifically, we employ the Fréchet Inception Distance (FID) (Heusel et al., 2017) to assess the image quality. We utilize the FVD_{16} and FVD_{32} scores, which calculate the Fréchet Video Distance (FVD) based on window sizes of 16 and 32 frames, respectively, to evaluate video quality across different temporal scales. Furthermore, we assess the perception loss of lip shape using the confidence score (LSE_C) and distance score (LSE_D) (Chung & Zisserman, 2017). To evaluate the preservation of speaker identity, we use ArcFace (Deng et al., 2019) to extract features from both the ground truth image and the generated image, and use the cosine similarity (CSIM) between the two as the evaluation metric. Moreover, we employ the Beat Align Score (BAS) (Siyao et al., 2022) to evaluate the synchronization of head motion and audio, and calculate the number of blinks per second (blink/s) to assess the liveliness of the eyes. **To better illustrate the error accumulation from a quantitative perspective, we design a metric to quantify the severity of error accumulation in the image space inspired by Bian et al. (2022) in the sequential generation task: Degradation Rate (DR), defined as $DR = \frac{FID_{ed}}{FID_{st}} - 1$. DR is related to the ratio between the FID of the last n frames FID_{ed} and the first n frames FID_{st} . The motivation for proposing this metric is that when error accumulation occurs, the quality of the generated data at the end of the sequence significantly deteriorates compared to the beginning. A larger DR indicates more severe error accumulation. In our experiments, we set n to 25 frames (1s) and 50 frames (2s), denoted as DR_{25} and DR_{50} , respectively.**

4.2 OVERALL COMPARISON

We compared our method with several state-of-the-art methods: Wav2Lip (Prajwal et al., 2020), Audio2Head (Wang et al., 2021), SadTalker (Zhang et al., 2023), Diffused Heads (Styplkowski et al., 2024), DreamTalk (Ma et al., 2023), Hallo (Xu et al., 2024b), and Echomimic (Chen et al., 2024). The quantitative experimental results are shown in Table 1. Our method achieves promising performance in FID, FVD_{16} , FVD_{32} , CSIM, BAS, and Blink/s metrics for the CREMA and HDTF datasets, as shown in Table 1. It also attains nearly best scores for LSE_C and LSE_D . **It is important to note that EchoMimic and DreamTalk are only applicable to face-aligned scenarios, whereas other methods do not require pre-cropping. Additionally, Hallo and EchoMimic are built upon pre-trained Stable Diffusion models (Rombach et al., 2022), inheriting substantial visual generation capabilities. Despite this, our method still achieves comparable or even better performance on the HDTF dataset. Furthermore, our method also outperforms Hallo and EchoMimic in terms of generation speed. In Appendix A.3.4, results indicate that our method achieves the fastest or near-fastest generation speed and requires significantly less time than Diffused Heads, Hallo, and Echomimic.**

For the qualitative experiment, as shown in Figure 2, we visualize the generation results for each baseline on different datasets. Our method evidently achieves the visual quality most similar to the ground truth, showcasing the most realistic and vivid visual effects. Compared to our method, SadTalker relies on the 3DMM prior, which limits its animation capability to the facial region only, resulting in significant artifacts when merging the face with the static torso below the neck. Additionally, SadTalker exhibits unnatural head pose movements and gaze direction, partially due to limited temporal modeling ability. Audio2Head fails to preserve the speaker’s identity during generation. For the HDTF dataset, the Diffused Heads method collapsed due to the error accumulation.

Table 1: Quantitative comparison with several state-of-the-art methods methods on HDTF (Zhang et al., 2021) and CREMA (Cao et al., 2014) datasets. We use **bold** to indicate the best score and underline to represent the second-best score. * Wav2Lip generated videos that only contain lip motions, while the rest remain still images. For the sake of rigor, we deem it as a reference for quality of lip motion and will not include Wav2Lip in the ranking. “ \uparrow ” indicates better performance with higher values, while “ \downarrow ” indicates better performance with lower values. For both BAS and Blink/s, we consider performance to be better when they are closer to the ground truth.

	Method	FID \downarrow	FVD $_{16}\downarrow$	FVD $_{32}\downarrow$	LSE $_C\uparrow$	LSE $_D\downarrow$	CSIM \uparrow	BAS	Blink/s
CREMA	GT	-	-	-	5.88	7.87	1	0.192	0.24
	Audio2Head	29.58	188.54	208.44	5.13	<u>7.92</u>	0.660	0.274	0.01
	SadTalker	16.05	101.43	158.85	<u>5.57</u>	7.36	<u>0.808</u>	0.244	0.33
	Diffused Heads	<u>13.01</u>	<u>64.27</u>	<u>116.18</u>	4.56	9.26	0.673	0.185	0.26
	Wav2Lip*	10.23	130.23	242.19	6.08	7.74	0.801	-	-
	DAWN (ours)	5.77	56.33	75.82	5.77	8.14	0.845	<u>0.231</u>	<u>0.29</u>
HDTF	GT	-	-	-	7.95	7.33	1	0.267	0.75
	Audio2Head	30.10	122.26	205.42	<u>6.88</u>	7.58	0.705	<u>0.290</u>	0.09
	SadTalker	26.11	97.43	187.43	6.27	8.03	<u>0.767</u>	<u>0.297</u>	<u>0.47</u>
	Wav2Lip*	23.85	166.15	281.73	7.42	7.44	0.701	-	-
	<u>DreamTalk</u>	58.8	406.58	516.21	6.48	8.43	0.641	0.311	0.032
	<u>Echomimic</u>	32.8	139.00	178.16	6.69	8.27	0.731	0.318	0.121
	<u>Hallo</u>	<u>14.2</u>	57.47	<u>100.99</u>	7.16	8.01	0.709	0.301	0.254
DAWN (ours)	9.60	<u>60.34</u>	95.64	6.71	<u>7.94</u>	0.790	0.281	0.86	

Table 2: Comparison with other generation strategies. The semi-autoregressive (SAR) generation strategy is similar to He et al. (2023). The two temporal resolution (TTR) generation method is mentioned in Harvey et al. (2022). For the DR metric, we consider the performance to be better when it is closer to zero.

Method	Time(s) \downarrow	FID \downarrow	FVD $_{16}\downarrow$	FVD $_{32}\downarrow$	LSE $_C\uparrow$	LSE $_D\downarrow$	DR $_{25}$	DR $_{50}$
SAR	11.42	13.00	120.33	210.52	4.34	8.29	0.307	0.021
TTR	19.25	9.77	95.42	137.14	4.87	8.68	-0.028	-0.005
Ours	7.32	9.60	60.34	95.64	6.71	7.94	0.044	0.031

DreamTalk is only applicable to face-aligned scenarios, thus requiring cropping the source image. Hallo causes serious error accumulation in the CREMA dataset, resulting in abnormal patches of color in the background, thus indicating the robustness defect.

4.3 COMPARISON WITH OTHER GENERATION STRATEGIES

We compared our non-autoregressive generation strategy with two regular video generation strategies: 1) semi-autoregressive (SAR) generation similar to He et al. (2023), and 2) two-temporal resolution (TTR), which trains two models with different temporal resolutions (Harvey et al., 2022). The time cost represents the time required to generate an 8-second talking head video. The models were evaluated on the CREMA dataset, and the results are shown in Table 2. According to the results, our non-autoregressive method produces videos with the highest overall quality and fastest speed. In addition, the SAR method results in a very high DR, which is at least one order of magnitude higher than TTR and NAR. This is because autoregressive methods suffer from degradation issues during iterative generation. Although TTR also successfully alleviates the degradation issue, it compromises generation speed and overall quality. In summary, our non-autoregressive method addresses the degradation problem while preserving fast generation speed and high overall quality.

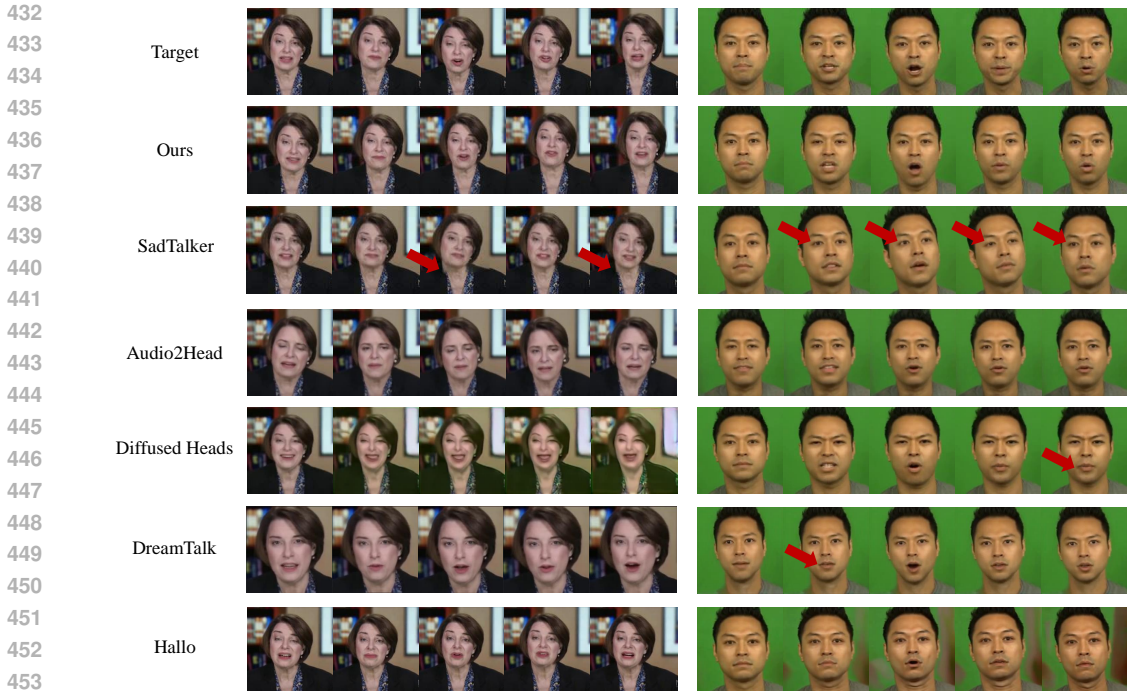


Figure 2: Qualitative comparison with several state-of-the-art methods on HDTF (Zhang et al., 2021) and CREMA (Cao et al., 2014) datasets. Our method produces higher-quality results in video quality, lip-sync consistency, identity preservation, and head motions.

Table 3: The experiment of extrapolation evaluation. "Inference length" refers to the number of frames generated in a single inference process.

Inference length	FID↓	FVD ₁₆ ↓	FVD ₃₂ ↓	LSE _C ↑	LSE _D ↓
40	9.35	59.58	94.09	5.76	7.89
100	9.83	61.72	98.80	6.41	7.96
200	9.60	60.34	95.64	6.71	7.94
400	10.36	61.57	97.84	6.63	8.12
600	10.30	60.44	96.62	6.76	8.02

4.4 EXTRAPOLATION VALIDATION

To evaluate the extrapolation ability of our method, we used the HDTF dataset to assess the impact of inference length on model performance, ranging from 40 to 600 frames. FID and FVD metrics remain stable with inference length, while longer audio improves lip movement precision. This suggests that inference with sufficient length helps the model produce more precise lip movement. Furthermore, to better compare the extrapolation of other DM-based methods using AR, Hallo was selected for comparison. As shown in Table A.3 from the Appendix A.3, the DR metric of our method stabilizes in a certain range, contrasting with Hallo’s error accumulation at increased inference lengths.

4.5 ABLATION STUDY

Ablation study on TCL strategy. Since TCL strategy is used only on A2V-FDM, PBNet is excluded by using ground truth pose/blink for evaluation. In this section, we extend the number of training epochs based on data throughput when using single-stage training. A2V-FDM trained with either stage 1 or 2 separately shows that stage 1 decreases overall performance except for FID, due to shorter clip training causing minor warping and lower FID scores but poorer FVD. Stage 2 improves LSE_C

Table 4: Ablation study on TCL and PBNet. The "GT PB" refers to whether to use ground truth pose/blink signal.

Method	GT PB	FID↓	FVD ₁₆ ↓	FVD ₃₂ ↓	LSE _C ↑	LSE _D ↓
only stage 1	✓	7.95	81.84	126.52	4.38	10.04
only stage 2	✓	13.71	125.75	166.83	6.14	8.43
DAWN	✓	9.68	52.05	87.11	6.71	7.99
w/o PBNet	×	15.20	100.94	162.35	5.79	8.36
DAWN	×	9.60	60.34	95.64	6.71	7.94

Table 5: User study.

Method	L-Sync	O-Nat	M-Viv	V-Qual
Audio2Head	3.87	3.67	3.28	3.66
Sadtalker	4.23	3.13	2.81	4.14
DreamTalk	4.38	3.89	3.41	4.42
Hallo	4.40	3.76	3.89	4.03
Echomimic	4.45	4.30	4.06	4.53
DAWN(ours)	4.57	4.41	4.43	4.51

and LSE_D but results in worse FID and FVD as the model struggles with simultaneous pose/blink control and lip movement. Both stages alone underperform compared to the proposed TCL strategy, underscoring its effectiveness.

Ablation study on PBNet. We evaluate the effectiveness of the PBNet in Table 4. The term "w/o PBNet" indicates that the PBNet module was removed from the architecture, requiring the A2V-FDM to simultaneously generate pose, blink, and lip motions from the audio by itself. The results suggest an overall enhancement of all evaluation metrics with the inclusion of PBNet. This is because modeling the long-term dependency of pose and blink movements through PBNet simplifies training for the A2V-FDM. We also visualized the effectiveness of PBNet in Appendix A.3.6.

4.6 USER STUDY

The user study evaluates generated videos across four dimensions: 1) L-Sync: Lip-audio synchronization; 2) O-Nat: The overall naturalness of the generated talking head; 3) M-Viv: The vividness of the head movements; 4) V-Qual: The overall video quality (e.g., presence of artifacts or abnormal color blocks). We generated 10 test videos per method, with 23 participants scoring each on a 1-5 scale. Users disregarded resolution and cropping when rating. As shown in Table 4.2, our method surpasses existing approaches in lip synchronization, naturalness, and head movement vividness, and is comparable to EchoMimic in video quality.

5 CONCLUSION

We introduce DAWN, an innovative architecture that non-autoregressively generates dynamic frames of talking head videos from given portraits and audio. We utilized the LFG to extract motion representations from speech videos. To produce vivid talking head videos, we propose PBNet and A2V-LDM. The PBNet generates natural pose/blink movements from speech, while A2V-LDM produces motion representations conditioned on audio and pose/blink movements. Finally, these generated motion representations are decoded into videos using LFG. We demonstrate on two datasets that our model can generate extended talking head videos with high-quality dynamic frames in a single pass, achieving realistic visual effects, accurate lip synchronization, and strong extrapolation capabilities.

REFERENCES

- 540
541
542 Yoshua Bengio, Jérôme Louradour, Ronan Collobert, and Jason Weston. Curriculum learning. In
543 *Proceedings of the 26th annual international conference on machine learning*, pp. 41–48, 2009.
- 544 Xiaohang Bian, Bo Qin, Xiaozhe Xin, Jianwu Li, Xuefeng Su, and Yanfeng Wang. Handwritten
545 mathematical expression recognition via attention aggregation based bi-directional mutual learning.
546 In *Proceedings of the AAAI conference on artificial intelligence*, volume 36, pp. 113–121, 2022.
- 547 Dan Bigioi, Shubhajit Basak, Michał Stypułkowski, Maciej Zieba, Hugh Jordan, Rachel McDonnell,
548 and Peter Corcoran. Speech driven video editing via an audio-conditioned diffusion model. *Image*
549 *and Vision Computing*, 142:104911, 2024.
- 550
551 Volker Blanz and Thomas Vetter. A morphable model for the synthesis of 3d faces. In *Proceedings*
552 *of the 26th Annual Conference on Computer Graphics and Interactive Techniques, SIGGRAPH*
553 *'99*, pp. 187–194, USA, 1999. ACM Press/Addison-Wesley Publishing Co. ISBN 0201485605.
554 doi: 10.1145/311535.311556. URL <https://doi.org/10.1145/311535.311556>.
- 555 Houwei Cao, David G Cooper, Michael K Keutmann, Ruben C Gur, Ani Nenkova, and Ragini Verma.
556 Crema-d: Crowd-sourced emotional multimodal actors dataset. *IEEE transactions on affective*
557 *computing*, 5(4):377–390, 2014.
- 558 Lele Chen, Guofeng Cui, Celong Liu, Zhong Li, Ziyi Kou, Yi Xu, and Chenliang Xu. Talking-head
559 generation with rhythmic head motion. In *European Conference on Computer Vision*, pp. 35–51.
560 Springer, 2020.
- 561 Zhiyuan Chen, Jiajiong Cao, Zhiquan Chen, Yuming Li, and Chenguang Ma. Echomimic: Lifelike
562 audio-driven portrait animations through editable landmark conditions, 2024. URL <https://arxiv.org/abs/2407.08136>.
- 563
564
565 Joon Son Chung and Andrew Zisserman. Out of time: automated lip sync in the wild. In *Computer*
566 *Vision—ACCV 2016 Workshops: ACCV 2016 International Workshops, Taipei, Taiwan, November*
567 *20-24, 2016, Revised Selected Papers, Part II 13*, pp. 251–263. Springer, 2017.
- 568 Özgün Çiçek, Ahmed Abdulkadir, Soeren S Lienkamp, Thomas Brox, and Olaf Ronneberger. 3d u-net:
569 learning dense volumetric segmentation from sparse annotation. In *Medical Image Computing and*
570 *Computer-Assisted Intervention—MICCAI 2016: 19th International Conference, Athens, Greece,*
571 *October 17-21, 2016, Proceedings, Part II 19*, pp. 424–432. Springer, 2016.
- 572 Jiankang Deng, Jia Guo, Niannan Xue, and Stefanos Zafeiriou. Arcface: Additive angular margin
573 loss for deep face recognition. In *Proceedings of the IEEE/CVF conference on computer vision*
574 *and pattern recognition*, pp. 4690–4699, 2019.
- 575
576 Chenpeng Du, Qi Chen, Tianyu He, Xu Tan, Xie Chen, Kai Yu, Sheng Zhao, and Jiang Bian.
577 Dae-talker: High fidelity speech-driven talking face generation with diffusion autoencoder. In
578 *Proceedings of the 31st ACM International Conference on Multimedia*, pp. 4281–4289, 2023.
- 579 Bo Fan, Lei Xie, Shan Yang, Lijuan Wang, and Frank K Soong. A deep bidirectional lstm approach
580 for video-realistic talking head. *Multimedia Tools and Applications*, 75:5287–5309, 2016.
- 581 Shiry Ginosar, Amir Bar, Gefen Kohavi, Caroline Chan, Andrew Owens, and Jitendra Malik. Learning
582 individual styles of conversational gesture. *CoRR*, abs/1906.04160, 2019. URL <http://arxiv.org/abs/1906.04160>.
- 583
584
585 Jianzhu Guo, Xiangyu Zhu, Yang Yang, Fan Yang, Zhen Lei, and Stan Z Li. Towards fast, accurate
586 and stable 3d dense face alignment. In *European Conference on Computer Vision*, pp. 152–168.
587 Springer, 2020.
- 588 Yudong Guo, Keyu Chen, Sen Liang, Yong-Jin Liu, Hujun Bao, and Juyong Zhang. Ad-nerf:
589 Audio driven neural radiance fields for talking head synthesis. In *Proceedings of the IEEE/CVF*
590 *international conference on computer vision*, pp. 5784–5794, 2021a.
- 591
592 Yudong Guo, Keyu Chen, Sen Liang, Yong-Jin Liu, Hujun Bao, and Juyong Zhang. Ad-nerf:
593 Audio driven neural radiance fields for talking head synthesis. In *Proceedings of the IEEE/CVF*
international conference on computer vision, pp. 5784–5794, 2021b.

- 594 William Harvey, Saeid Naderiparizi, Vaden Masrani, Christian Weillbach, and Frank
595 Wood. Flexible diffusion modeling of long videos. In S. Koyejo, S. Mohamed,
596 A. Agarwal, D. Belgrave, K. Cho, and A. Oh (eds.), *Advances in Neural Infor-*
597 *mation Processing Systems*, volume 35, pp. 27953–27965. Curran Associates, Inc.,
598 2022. URL [https://proceedings.neurips.cc/paper_files/paper/2022/](https://proceedings.neurips.cc/paper_files/paper/2022/file/b2fe1ee8d936ac08dd26f2ff58986c8f-Paper-Conference.pdf)
599 [file/b2fe1ee8d936ac08dd26f2ff58986c8f-Paper-Conference.pdf](https://proceedings.neurips.cc/paper_files/paper/2022/file/b2fe1ee8d936ac08dd26f2ff58986c8f-Paper-Conference.pdf).
- 600
601 Tianyu He, Junliang Guo, Runyi Yu, Yuchi Wang, Jialiang Zhu, Kaikai An, Leyi Li, Xu Tan, Chunyu
602 Wang, Han Hu, et al. Gaia: Zero-shot talking avatar generation. *arXiv preprint arXiv:2311.15230*,
603 2023.
- 604 Martin Heusel, Hubert Ramsauer, Thomas Unterthiner, Bernhard Nessler, and Sepp Hochreiter. Gans
605 trained by a two time-scale update rule converge to a local nash equilibrium. *Advances in neural*
606 *information processing systems*, 30, 2017.
- 607
608 Jonathan Ho, Ajay Jain, and Pieter Abbeel. Denoising diffusion probabilistic models. *Advances in*
609 *neural information processing systems*, 33:6840–6851, 2020.
- 610
611 Jonathan Ho, William Chan, Chitwan Saharia, Jay Whang, Ruiqi Gao, Alexey Gritsenko, Diederik P
612 Kingma, Ben Poole, Mohammad Norouzi, David J Fleet, et al. Imagen video: High definition
613 video generation with diffusion models. *arXiv preprint arXiv:2210.02303*, 2022a.
- 614
615 Jonathan Ho, Tim Salimans, Alexey Gritsenko, William Chan, Mohammad Norouzi, and David J
616 Fleet. Video diffusion models. *Advances in Neural Information Processing Systems*, 35:8633–8646,
617 2022b.
- 618
619 Fa-Ting Hong, Longhao Zhang, Li Shen, and Dan Xu. Depth-aware generative adversarial network
620 for talking head video generation. In *Proceedings of the IEEE/CVF conference on computer vision*
621 *and pattern recognition*, pp. 3397–3406, 2022.
- 622
623 Wei-Ning Hsu, Benjamin Bolte, Yao-Hung Hubert Tsai, Kushal Lakhotia, Ruslan Salakhutdinov,
624 and Abdelrahman Mohamed. Hubert: Self-supervised speech representation learning by masked
625 prediction of hidden units. *IEEE/ACM transactions on audio, speech, and language processing*,
626 29:3451–3460, 2021.
- 627
628 Phillip Isola, Jun-Yan Zhu, Tinghui Zhou, and Alexei A. Efros. Image-to-image translation with
629 conditional adversarial networks. *CoRR*, abs/1611.07004, 2016a. URL [http://arxiv.org/](http://arxiv.org/abs/1611.07004)
630 [abs/1611.07004](http://arxiv.org/abs/1611.07004).
- 631
632 Phillip Isola, Jun-Yan Zhu, Tinghui Zhou, and Alexei A. Efros. Image-to-image translation with
633 conditional adversarial networks. *2017 IEEE Conference on Computer Vision and Pattern Recog-*
634 *nition (CVPR)*, pp. 5967–5976, 2016b. URL [https://api.semanticscholar.org/](https://api.semanticscholar.org/CorpusID:6200260)
635 [CorpusID:6200260](https://api.semanticscholar.org/CorpusID:6200260).
- 636
637 Xinya Ji, Hang Zhou, Kaisiyuan Wang, Qianyi Wu, Wayne Wu, Feng Xu, and Xun Cao. Eamm: One-
638 shot emotional talking face via audio-based emotion-aware motion model. In *ACM SIGGRAPH*
639 *2022 Conference Proceedings*, pp. 1–10, 2022.
- 640
641 Justin Johnson, Alexandre Alahi, and Li Fei-Fei. Perceptual losses for real-time style transfer
642 and super-resolution. *CoRR*, abs/1603.08155, 2016. URL [http://arxiv.org/abs/1603.](http://arxiv.org/abs/1603.08155)
643 [08155](http://arxiv.org/abs/1603.08155).
- 644
645 Diederik P Kingma and Max Welling. Auto-encoding variational bayes, 2022. URL [https:](https://arxiv.org/abs/1312.6114)
646 [//arxiv.org/abs/1312.6114](https://arxiv.org/abs/1312.6114).
- 647
648 Yunfei Liu, Lijian Lin, Fei Yu, Changyin Zhou, and Yu Li. Moda: Mapping-once audio-driven
649 portrait animation with dual attentions. In *Proceedings of the IEEE/CVF International Conference*
650 *on Computer Vision*, pp. 23020–23029, 2023.
- 651
652 Minh-Thang Luong. Effective approaches to attention-based neural machine translation. *arXiv*
653 *preprint arXiv:1508.04025*, 2015.

- 648 Yifeng Ma, Shiwei Zhang, Jiayu Wang, Xiang Wang, Yingya Zhang, and Zhidong Deng. Dreamtalk:
649 When expressive talking head generation meets diffusion probabilistic models. *arXiv preprint*
650 *arXiv:2312.09767*, 2023.
- 651
- 652 Arsha Nagrani, Joon Son Chung, and Andrew Senior. Voxceleb: A large-scale speaker identifica-
653 tion dataset. In *Interspeech 2017*. ISCA, August 2017. doi: 10.21437/interspeech.2017-950. URL
654 <http://dx.doi.org/10.21437/Interspeech.2017-950>.
- 655
- 656 Haomiao Ni, Changhao Shi, Kai Li, Sharon X. Huang, and Martin Renqiang Min. Conditional
657 image-to-video generation with latent flow diffusion models, 2023. URL <https://arxiv.org/abs/2303.13744>.
- 658
- 659 Alexander Quinn Nichol and Prafulla Dhariwal. Improved denoising diffusion probabilistic models.
660 In *International conference on machine learning*, pp. 8162–8171. PMLR, 2021.
- 661
- 662 William Peebles and Saining Xie. Scalable diffusion models with transformers. In *Proceedings of*
663 *the IEEE/CVF International Conference on Computer Vision*, pp. 4195–4205, 2023.
- 664
- 665 Mathis Petrovich, Michael J. Black, and Gül Varol. Action-conditioned 3d human motion synthesis
666 with transformer VAE. *CoRR*, abs/2104.05670, 2021. URL <https://arxiv.org/abs/2104.05670>.
- 667
- 668 KR Prajwal, Rudrabha Mukhopadhyay, Vinay P Nambodiri, and CV Jawahar. A lip sync expert is
669 all you need for speech to lip generation in the wild. In *Proceedings of the 28th ACM international*
670 *conference on multimedia*, pp. 484–492, 2020.
- 671
- 672 Albert Pumarola, Antonio Agudo, Aleix M. Martinez, Alberto Sanfeliu, and Francesc Moreno-Noguer.
673 Ganimation: Anatomically-aware facial animation from a single image. In *Proceedings of the*
674 *European Conference on Computer Vision (ECCV)*, September 2018.
- 675
- 676 Haonan Qiu, Menghan Xia, Yong Zhang, Yingqing He, Xintao Wang, Ying Shan, and Ziwei
677 Liu. Freenoise: Tuning-free longer video diffusion via noise rescheduling. *arXiv preprint*
arXiv:2310.15169, 2023.
- 678
- 679 Yurui Ren, Ge Li, Yuanqi Chen, Thomas H Li, and Shan Liu. Pirenderer: Controllable portrait
680 image generation via semantic neural rendering. In *Proceedings of the IEEE/CVF international*
681 *conference on computer vision*, pp. 13759–13768, 2021.
- 682
- 683 Robin Rombach, Andreas Blattmann, Dominik Lorenz, Patrick Esser, and Björn Ommer. High-
684 resolution image synthesis with latent diffusion models. In *Proceedings of the IEEE/CVF confer-*
ence on computer vision and pattern recognition, pp. 10684–10695, 2022.
- 685
- 686 Shuai Shen, Wenliang Zhao, Zibin Meng, Wanhua Li, Zheng Zhu, Jie Zhou, and Jiwen Lu. Diff-
687 talk: Crafting diffusion models for generalized audio-driven portraits animation. In *Proceedings of the*
688 *IEEE/CVF Conference on Computer Vision and Pattern Recognition*, pp. 1982–1991, 2023.
- 689
- 690 Aliaksandr Siarohin, Stéphane Lathuilière, Sergey Tulyakov, Elisa Ricci, and Nicu Sebe. First order
691 motion model for image animation. *CoRR*, abs/2003.00196, 2020. URL <https://arxiv.org/abs/2003.00196>.
- 692
- 693 Aliaksandr Siarohin, Oliver J. Woodford, Jian Ren, Menglei Chai, and Sergey Tulyakov. Motion
694 representations for articulated animation. *CoRR*, abs/2104.11280, 2021. URL <https://arxiv.org/abs/2104.11280>.
- 695
- 696 Li Siyao, Weijiang Yu, Tianpei Gu, Chunze Lin, Quan Wang, Chen Qian, Chen Change Loy, and
697 Ziwei Liu. Bailando: 3d dance generation by actor-critic gpt with choreographic memory. In
698 *Proceedings of the IEEE/CVF Conference on Computer Vision and Pattern Recognition*, pp.
699 11050–11059, 2022.
- 700
- 701 Jiaming Song, Chenlin Meng, and Stefano Ermon. Denoising diffusion implicit models. *arXiv*
preprint arXiv:2010.02502, 2020.

- 702 Michał Stypułkowski, Konstantinos Vougioukas, Sen He, Maciej Zięba, Stavros Petridis, and Maja
703 Pantic. Diffused heads: Diffusion models beat gans on talking-face generation. In *Proceedings of*
704 *the IEEE/CVF Winter Conference on Applications of Computer Vision*, pp. 5091–5100, 2024.
- 705
706 Jianlin Su, Yu Lu, Shengfeng Pan, Ahmed Murtadha, Bo Wen, and Yunfeng Liu. Roformer: Enhanced
707 transformer with rotary position embedding, 2023. URL [https://arxiv.org/abs/2104.](https://arxiv.org/abs/2104.09864)
708 09864.
- 709 Linrui Tian, Qi Wang, Bang Zhang, and Liefeng Bo. Emo: Emote portrait alive-generating expres-
710 sive portrait videos with audio2video diffusion model under weak conditions. *arXiv preprint*
711 *arXiv:2402.17485*, 2024.
- 712
713 Konstantinos Vougioukas, Stavros Petridis, and Maja Pantic. Realistic speech-driven facial animation
714 with gans. *International Journal of Computer Vision*, 128(5):1398–1413, 2020.
- 715
716 Suzhen Wang, Lincheng Li, Yu Ding, Changjie Fan, and Xin Yu. Audio2head: Audio-driven one-shot
717 talking-head generation with natural head motion. *arXiv preprint arXiv:2107.09293*, 2021.
- 718
719 Weihao Xia, Yulun Zhang, Yujiu Yang, Jing-Hao Xue, Bolei Zhou, and Ming-Hsuan Yang. Gan
720 inversion: A survey. *IEEE transactions on pattern analysis and machine intelligence*, 45(3):
721 3121–3138, 2022.
- 722
723 Chao Xu, Yang Liu, Jiazheng Xing, Weida Wang, Mingze Sun, Jun Dan, Tianxin Huang, Siyuan Li,
724 Zhi-Qi Cheng, Ying Tai, et al. Facechain-imagineid: Freely crafting high-fidelity diverse talking
725 faces from disentangled audio. In *Proceedings of the IEEE/CVF Conference on Computer Vision*
726 *and Pattern Recognition*, pp. 1292–1302, 2024a.
- 727
728 Mingwang Xu, Hui Li, Qingkun Su, Hanlin Shang, Liwei Zhang, Ce Liu, Jingdong Wang, Yao Yao,
729 and Siyu Zhu. Hallo: Hierarchical audio-driven visual synthesis for portrait image animation,
730 2024b. URL <https://arxiv.org/abs/2406.08801>.
- 731
732 Sicheng Xu, Guojun Chen, Yu-Xiao Guo, Jiaolong Yang, Chong Li, Zhenyu Zang, Yizhong Zhang,
733 Xin Tong, and Baining Guo. Vasa-1: Lifelike audio-driven talking faces generated in real time.
734 *arXiv preprint arXiv:2404.10667*, 2024c.
- 735
736 Wenxuan Zhang, Xiaodong Cun, Xuan Wang, Yong Zhang, Xi Shen, Yu Guo, Ying Shan, and Fei
737 Wang. Sadtalker: Learning realistic 3d motion coefficients for stylized audio-driven single image
738 talking face animation. In *Proceedings of the IEEE/CVF Conference on Computer Vision and*
739 *Pattern Recognition*, pp. 8652–8661, 2023.
- 740
741 Zhimeng Zhang, Lincheng Li, Yu Ding, and Changjie Fan. Flow-guided one-shot talking face
742 generation with a high-resolution audio-visual dataset. In *Proceedings of the IEEE/CVF Conference*
743 *on Computer Vision and Pattern Recognition*, pp. 3661–3670, 2021.
- 744
745 Hang Zhou, Yasheng Sun, Wayne Wu, Chen Change Loy, Xiaogang Wang, and Ziwei Liu. Pose-
746 controllable talking face generation by implicitly modularized audio-visual representation. In
747 *Proceedings of the IEEE/CVF conference on computer vision and pattern recognition*, pp. 4176–
748 4186, 2021.
- 749
750 Yang Zhou, Xintong Han, Eli Shechtman, Jose Echevarria, Evangelos Kalogerakis, and Dingzeyu Li.
751 Makelttalk: speaker-aware talking-head animation. *ACM Transactions On Graphics (TOG)*, 39(6):
752 1–15, 2020.
- 753
754
755

A APPENDIX

A.1 SOCIAL IMPACT CONSIDERATION

DAWN focuses on creating realistic talking head videos with the aim of generating positive social impact. We firmly oppose the malicious misuse of our method, including fraud, creating fake news, and violating portrait rights. Thus, we assert that our open-source code and model should be used exclusively for research purposes. We hope that our technique can provide social benefits in the future, such as promoting education, enabling face-to-face communication for separated people, and treating certain psychological disorders.

A.2 TRAINING DETAILS

Since the HDTF dataset contains fewer videos of longer length compared to the CREMA dataset, each video in the HDTF dataset is sampled 25 times per epoch to achieve better I/O performance. The LFG is fine-tuned independently on the training datasets of CREMA and HDTF, using a checkpoint initially trained on the VoxCeleb (Nagrani et al., 2017) dataset. We fine-tune the LFG with 400 epochs. During the training of A2V-FDM, we trained with 500 epochs for each stage. In both two stages, we select the $w_{lip} = 1$ for the loss function in Equation 7. We freeze the parameters of LFG when training the A2V-FDM. Although end-to-end training can prevent errors in the LFG from affecting the A2V-FDM, the primary reason we did not adopt an end-to-end training approach is the difficulty in achieving stable convergence. In an end-to-end training setup, the A2V-FDM is likely to receive incorrect supervision signals, which can hinder the training process of the model and make it highly unstable. For PBNet, the MSE-based reconstruction loss can be expressed as:

$$\mathcal{L}_{\text{MSE}} = \frac{1}{T} \sum_{n=1}^N (\Delta \hat{\rho}_n - \Delta \rho_n)^2 \quad (11)$$

where $\Delta \hat{\rho}$ is the predicted pose/blink sequences, and $\Delta \rho$ is the ground truth sequences. We also implement a KL divergence loss to constrain the latent code \mathbf{h} closely approximates a standard Gaussian distribution. The adversarial loss L_{GAN} is defined as:

$$L_{\text{GAN}} = \arg \min_G \max_D (G, D) \quad (12)$$

where the G is our proposed PBNet and the D is a discriminator implemented based on PatchGAN (Isola et al., 2016b). We use a 1D convolution based network to output the probability of each patch in the pose/blink sequence originating from real actions. The discriminator is guided by the BCE loss. In the training, the loss function of PBNet is set as:

$$L = \lambda_{\text{rec}} L_{\text{rec}} + \lambda_{\text{KL}} L_{\text{KL}} + \lambda_{\text{GAN}} L_{\text{GAN}} \quad (13)$$

where we set $\lambda_{\text{rec}} = 1$, $\lambda_{\text{GAN}} = 0.6$. During the training process, we observed that L_{KL} rapidly converges to approximately zero at the beginning. This convergence impairs the latent state’s ability to retain effective information, causing the model to depend almost entirely on the decoder’s predictive capability for completing the fixed fitting task from audio to pose/blink. To ensure diversity in generation, we implemented a method of progressively increasing the λ_{KL} in training PBNet. The PBNet was trained over 1600 epochs. In the initial 400 epochs, we did not apply the L_{KL} constraint to the latent code., which helped the model develop basic sequence reconstruction capabilities in the early training phase. From that point until the end of training, λ_{KL} was gradually increased to 0.01.

A.3 ADDITIONAL EXPERIMENTS

A.3.1 EXTRAPOLATION COMPARISON

To highlight the advantages of NAR generation, we selected an image-based diffusion method, Hallo, for comparison, due to its representative structure similar to most of the latest AR or SAR methods. We evaluated the degradation rate for both our model and Hallo across inference lengths of 200, 400,

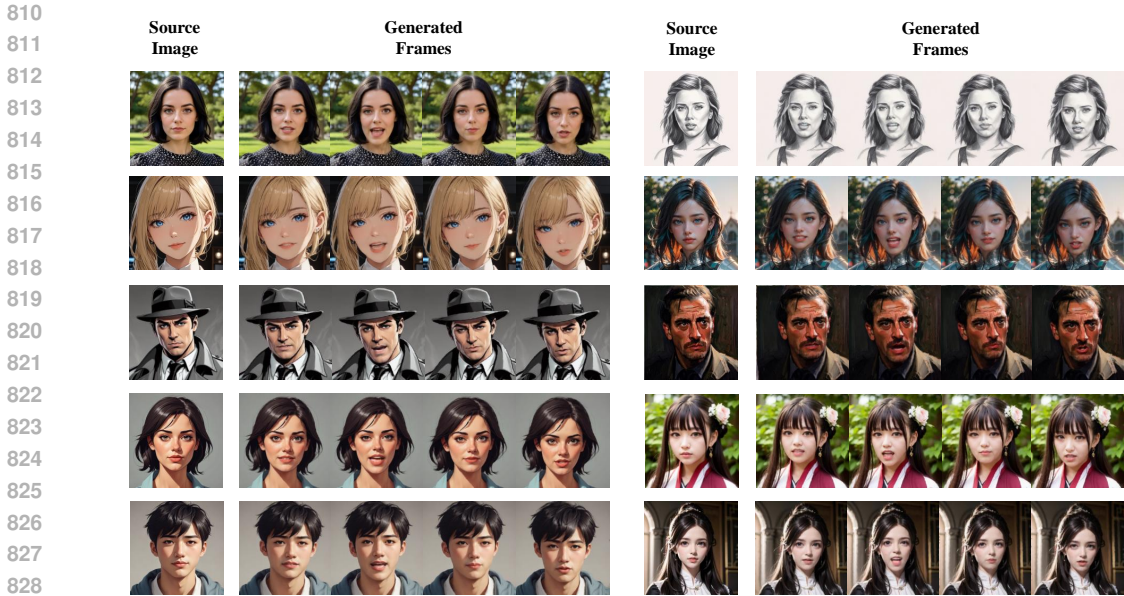


Figure 3: The qualitative study on higher resolution (256×256) and different portrait styles.

Table 6: The comparison experiment of error accumulation with Hallo. "Inference length" refers to the number of frames generated in a single inference process.

Inference length	DAWN		Hallo	
	DR ₂₅	DR ₅₀	DR ₂₅	DR ₅₀
200	0.253	0.043	0.214	0.094
400	0.208	0.164	0.279	0.161
600	0.152	0.152	0.422	0.332

and 600, as detailed in Table A.3. The results indicate that, in our method, both the DR₂₅ and DR₅₀ metrics remain stable as inference length increases. In contrast, Hallo’s DR₂₅ and DR₅₀ metrics significantly increase with longer inference lengths, suggesting notable error accumulation in the image space. This demonstrates that image-based AR methods, such as Hallo, struggle with error accumulation in longer tasks, while our model exhibits superior extrapolation capabilities and more consistent performance with extended video sequences. These findings underscore the superiority of NAR methods compared to AR and SAR alternatives.

A.3.2 POSE/BLINK CONTROLLABLE GENERATION

In addition to generating lifelike avatars, our method also enables the controllable generation of pose and blink actions. Users can either use pose and blink information generated by our PBNNet or provide these sequences directly, such as by extracting them from a given video. The results, as shown in Figure 4, demonstrate that our method not only provides high-precision control over the pose/blink movements of the generated avatars, but also effectively transfers rich facial dynamics, including expressions, blinks, and lip motions.

A.3.3 EXPERIMENT ON HIGHER RESOLUTION AND DIFFERENT PORTRAIT STYLES

We further investigate the generalization ability of our method on higher-resolution images and different portrait styles. We trained DAWN on the HDTF dataset with a resolution of 256×256 . Then we evaluated our higher-resolution model on the HDTF test set. The quantitative results are

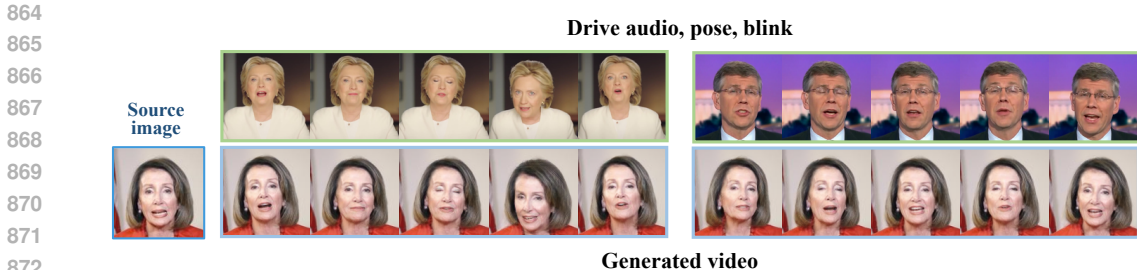


Figure 4: Visualization of cross-identity reenactment. We extract the audio, head pose, and blink signals from the video in the first row, and use them to drive the source image, generating the talking head video in the second row.

Table 7: Quantitative study on different resolutions. The "128" indicates our method is trained on a 128×128 resolution, and the "256" indicates training on a 256×256 resolution.

Method	FID↓	FVD ₁₆ ↓	FVD ₃₂ ↓	LSE _C ↑	LSE _D ↓	CSIM↑	BAS	Blink/s
GT	-	-	-	7.95	7.33	1	0.267	0.75
DAWN (128)	9.60	60.34	95.64	6.71	7.94	0.790	0.281	0.86
DAWN (256)	11.80	68.07	105.20	7.20	7.80	0.791	0.278	0.73

illustrated in Table A.3.4. The results show that our method still maintains strong competitiveness compared to the latest talking head models. We also test our method on multiple out-of-dataset source images featuring diverse styles, as showcased in Figure 3. The results indicate that our method yields promising outcomes in high-resolution generation and demonstrates considerable generalization ability across various image styles, including photos, paintings, anime, and sketches.

A.3.4 COMPARISON EXPERIMENT ON GENERATION TIME COST

We experimented to test the time cost of video generation. We generated 8-second talking head videos with the same source image and audio, then recorded the time consumption for each method. To ensure a fair comparison, we excluded the audio encoding step for all methods. The testing was performed on a single V100 16G GPU. As shown in Figure A.3.4, our method achieves the fastest or near-fastest generation speed and requires significantly less time compared to the previous diffusion-based methods, Diffused Heads, Hallo, and Echomimic.

A.3.5 ABLATION STUDY ON THE LOCAL ATTENTION MECHANISM

In our work, we utilized a local attention mechanism to enhance the extrapolation capability of our model. We conducted experiments to evaluate the effect of varying the window size of the local attention mechanism in A2V-FDM, ranging from 20 to 200, and also assessed the model’s performance without the local attention mechanism. To eliminate the influence of the generated pose/blink, we used the ground-truth pose/blink signals to drive the model. The results, presented in Table 8, indicate that the model’s performance peaks around a window size of 80. This is attributed to the maximum length of the video clips during training, which is 40 frames. Consequently, the model learns to process temporal dependencies within a 40-frame distance. Thus, using the window size of twice the max training clip length takes full advantage of the model’s capability. Reducing or increasing the window size degrades performance; a smaller window size leads to a loss of contextual information, significantly impairing the model’s performance, while a larger window size or the absence of the local attention mechanism reduces extrapolation ability, also resulting in lower performance. Since extrapolation ability is also supported by our TCL strategy and the intrinsic structure of A2V-FDM, removing the local attention mechanism causes relatively minor damage compared to the loss of contextual information.

918
919
920
921
922
923
924
925
926
927
928
929
930
931
932
933
934
935
936
937
938
939
940
941
942
943
944
945
946
947
948
949
950
951
952
953
954
955
956
957
958
959
960
961
962
963
964
965
966
967
968
969
970
971

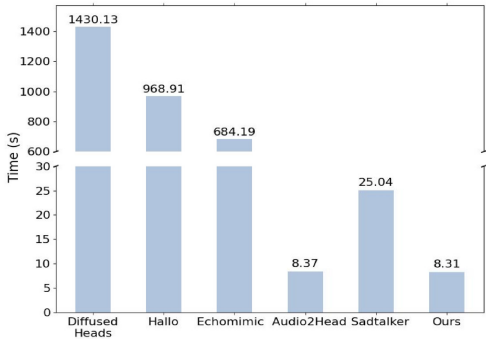


Figure 5: The comparison experiment on generation time cost. The Diffused Heads, Hallo, Echomimic are existing diffusion-based methods.

Table 8: Ablation study on the local attention mechanism. The "window" means the window size in the local attention operation. The "None" means we use the original attention mechanism instead.

Window	FID↓	FVD ₁₆ ↓	FVD ₃₂ ↓	LSE _C ↑	LSE _D ↓
20	14.47	159.19	217.54	5.69	8.97
40	10.93	72.93	114.52	6.35	8.33
80	9.68	52.05	87.11	6.71	7.99
200	9.44	53.48	88.84	6.60	7.94
None	9.70	63.95	103.83	6.37	8.15

A.3.6 ABLATION STUDY ON THE PBNET

We further provide the visualization of the ablation study on PBNet in Figure 6, while the quantitative results are illustrated in Table 4. It suggests that using the PBNet to generate the pose exclusively will provide the pose with more vividness and diversity. However, generating lip, head pose, and blink movement from audio simultaneously will cause a relatively static head pose, which severely impacts the vividness and naturalness.

A.3.7 ABLATION STUDY ON THE PBNET

A.4 LIMITATION AND FUTURE WORKS

Our work still has certain limitations. For instance, the model cannot fully comprehend the physical common sense during the generation, particularly when individuals in the portraits wearing items such as hats, helmets or headpieces. Sometimes, these items will not move along with the head, thus causing artifacts in the results. We leave the injection of these physical dependencies into the model without the loss of vividness as our future work. **Additionally, our architecture currently requires training each sub-module separately. In future work, we plan to enable joint training to minimize error propagation across different modules.**

972
973
974
975
976
977
978
979
980
981
982
983
984
985
986
987
988
989
990
991
992
993
994
995
996
997
998
999
1000
1001
1002
1003
1004
1005
1006
1007
1008
1009
1010
1011
1012
1013
1014
1015
1016
1017
1018
1019
1020
1021
1022
1023
1024
1025



Figure 6: The visualization of the ablation study on PBNet demonstrates different methodologies. The term "w/o PBNet" indicates "without PBNet", whereby the A2V-FDM is utilized to infer pose and blink movements. Conversely, "w PBNet" signifies the "with PBNet", which directly generates explicit pose and blink signals to control the generation of A2V-FDM.